Pyrolysis activation energy of cellulosic fibres investigated by a method derived from the first order global model

Yunhao Liang, Michael E. Ries[*], Peter J. Hine

School of Physics and Astronomy, University of Leeds, Woodhouse Lane, Leeds LS2 9JT, UK

ABSTRACT

The pyrolysis kinetics of cellulosic fibres, a natural cotton yarn (NCY) and a mercerized cotton yarn (MCY), has been explored with a modified first order global analysis method (FOG), via a series of non-isothermal experiments, using thermogravimetric analysis (TGA). The modified FOG analysis routine was developed to overcome discrepancy in heating rate and the difference between exact results and approximations in integrals. The intrinsic pyrolysis activation energy, with temperature range tending to zero, was found to be independent of heating rate and approximation used, giving average values of 153 ± 2 kJ/mol for NCY and 192 ± 7 kJ/mol for MCY. This proves the applicability of the reported analysis routine under the conducted TGA measurements. The reasons for different values were hypothesized to be the difference in chemical composition and crystalline structure. The findings provide a new approach in the investigation on pyrolysis kinetics of biomass and factors impacting their pyrolytic behaviour.

1. Introduction

Extensive attention has been focussed on biomass energy of which cellulose is the most abundant biopolymer on the earth (Qu, He, Cai, Huang, & Ning, 2016; Shen, Gu, & Bridgwater, 2010; Yaman, 2004; Zhang et al., 2010). The thermochemical conversion is one of the most common methods to harvest the energy stored in cellulose-based materials. Pyrolysis kinetics is used to investigate how the materials behave under elevated temperatures, which can help reveal the reaction mechanism underlying thermochemical utilization processes, prediction of reaction rates and difficulty of thermoregulation.

The kinetic research on the pyrolysis of cellulose-based materials can be traced back to the 1950s (Stamm, 1956). In this research field, two measurements can be applied, isothermal (Chen & Kuo, 2011) and non-isothermal (Yue et al., 2012). Due to the relatively low heating rate of most TGA apparatus, cellulose samples can be significantly degraded before the required temperature is reached during an isothermal process, giving difficulty to reach the ideal isothermal conditions. Therefore, non-isothermal methods are commonly used in terms of the research on the pyrolysis of cellulose-based materials (Wang, Dai, Yang, & Luo, 2017) Although pyrolysis is a thermally stimulated heterogeneous reaction, the theories of the kinetic model are mostly developed from those of homogeneous reaction kinetics (Şerbănescu, 2014). The

conversion, α, expresses how much of the organic substance is pyrolyzed and it can be calculated from the initial sample weight (w_o), the initial water content (w_{H_2O}), the sample weight at time t (w_t), and the residual char weight (w_∞) via Eq. (1) (Broido, 1969). The reaction rate can then be expressed by Eq. (2) (Coats & Redfern, 1964; Wang et al., 2017)

$$\alpha = \frac{w_o - w_{H_2O} - w_t}{w_o - w_{H_2O} - w_\infty} \tag{1}$$

$$\frac{d\alpha}{dt} = k(T)f(\alpha) \tag{2}$$

where the rate constant $k(T)$ can be described with an Arrhenius theory (Eq. (3)), of which A and E are the frequency factor and the pyrolysis activation energy respectively; and $f(\alpha)$ is a chosen reaction model, with reaction order to be n, and is generally written as Eq. (4) (Coats & Redfern, 1964; Wang et al., 2017).

$$k(T) = A exp\left(-\frac{E}{RT}\right) \tag{3}$$

$$f(\alpha) = (1 - \alpha)^n \tag{4}$$

As for the non-isothermal measurements, linear heating methods with a heating rate of β as expressed by Eq. (5) are used and are within

the scope of this research.

$$T = T_o + \beta t \tag{5}$$

where T_o and t are the initial temperature and the evolving time, respectively.

By combining the equations above, Eq. (2) can be rewritten as:

$$\frac{d\alpha}{dt} = \frac{d\alpha}{dT}\frac{dT}{dt} = \frac{d\alpha}{dT}\beta = A exp\left(-\frac{E}{RT}\right)(1-\alpha)^n \tag{6}$$

Among the non-isothermal measurements, two methods are most readily used: the model-fitting method and the so-called "model-free" method. For the former, the reaction model, $f(\alpha)$, is assumed in advance and then fitted to the experimental data to obtain the kinetic parameters, such as the Coats-Redfern integration method (Coats & Redfern, 1964). The first order global model (FOG), where n in Eq. (4) is unity, has been used intensively for cellulose pyrolysis (Şerbănescu, 2014). It is considered as satisfactorily describing the process at linear heating rates up to 100 °C/min and the kinetics can be represented by this single-step process (Banyasz, Li, Lyons-Hart, & Shafer, 2001; Şerbănescu, 2014). For the model-free methods, they are based on the principle that the reaction speed is only a function of temperature at constant conversion, also called the isoconversional method, and does not need the prior assumption of the form of $f(\alpha)$. The kinetic parameters, activation energy and pre-factor, can be determined from a series of TGA tests carried out with different heating rates, normally at least three rates (Friedman, 1964; Şerbănescu, 2014). There are two categories of isoconversional methods: differential methods and integral methods. Due to the fact that no approximations are required, which could lead to discrepancies of the temperature integral, and there is no requirement on the prior assumption of $f(\alpha)$, then the differential methods on the same equations are theoretically more reliable than the integral methods (Wang et al., 2017). The Friedman method is one of the most commonly used differential methods (Wang et al., 2017), and it can be expressed by:

$$ln\left(\frac{d\alpha}{dt}\right) = ln\left(\frac{d\alpha}{dT}\frac{dT}{dt}\right) = ln\left(\beta\frac{d\alpha}{dT}\right) = ln[Af(\alpha)] - \frac{E}{R}*\frac{1}{T} \tag{7}$$

The reported pyrolysis activation energy ranges of cellulose, hemicellulose and lignin are summarized in Table 1. Their decomposition temperatures range from 220 to 315 °C for hemicellulose, from 300 to 400 °C for cellulose and from 150 to 900 °C for lignin (Leng et al., 2022; Lv et al., 2010; Yang, Yan, Chen, Lee, & Zheng, 2007). In other words, the hemicellulose is less thermally stable than cellulose, and lignin has the widest thermal degradation temperature range among them. It has

Table 1
A summary of the reported pyrolysis activation energies of cellulose, hemicellulose and lignin from literature.

Material	Pyrolysis activation energy range (kJ/mol)	Reference
Cellulose	135–223	(Cao, Li, Martí-Rosselló, & Zhang, 2019; Fan et al., 2017; Luo et al., 2020; Mamleev, Bourbigot, & Yvon, 2007; Morgado & Frollini, 2011; Özsin, 2020; Yeo, Chin, Tan, & Loh, 2019; Zhang et al., 2022; Zhu & Zhong, 2020)
Hemicellulose	115–144	(Cao et al., 2019; Ding et al., 2020; Moriana, Zhang, Mischnick, Li, & Ek, 2014; Thanatawee, Rukthong, Sunphorka, Piumsomboon, & Chalermsinsuwan, 2016; Yeo et al., 2019; Zhang et al., 2022; Zhu & Zhong, 2020)
Lignin	23–243	(Cao et al., 2019; Dussan, Dooley, & Monaghan, 2019; Farag, Attia, & Mohaddespour, 2021; Thanatawee et al., 2016; Yeo et al., 2019; Zhang et al., 2022; Zhu & Zhong, 2020)

been reported that the crystallinity/crystalline size (Kim, Eom, & Wada, 2010; Poletto, Zattera, Forte, & Santana, 2012), chemical composition (Ramiah, 1970; Zhu & Zhong, 2020) and degree of polymerization (Vanderfleet et al., 2019) can also influence the thermal stability of lignocellulose in a complex way. For this reason, these two aspects, chemical composition and crystal structure, are explored in this work by investigating a natural cotton yarn (NCY) and a mercerized cotton yarn (MCY).

Even though the effect of lag in heat transfer, i.e. the difference between the external temperature and the internal temperature, on the pyrolysis kinetics parameters has been reported (Czajka, 2021), the influence of the difference between the actual heating speed and the target heating speed on a TGA machine is rarely considered. This can influence the validity of the assumption addressed from those models, i.e. the heating rate is assumed to be constant which can be not quite true in reality and so this is also investigated in the study.

This research presented in this paper investigates the pyrolysis behaviour with a modified model derived from the well-known first order global method. The important aspect from the reliability of the TGA machine in terms of the heating rate is also analysed. Further, the pyrolysis behaviour of the two cotton samples is compared in association with the other characteristics of the samples, such as molecular weight, carbohydrate composition and crystalline structure. We hypothesize that the chemical composition and/or crystalline structure dominate the pyrolysis kinetics.

2. Materials and methods

2.1. Materials

The cellulose sources are from two undyed cotton yarns, a natural cotton yarn (NCY) (obtained from Airedale Yarns, Keighley, UK) and a mercerized cotton yarn (MCY) (100 m-nr50, No. 1716, Coats Group plc, UK), and they were used as received. The mercerization process is an industrial process often used for cotton fibres to increase the adhesion of dyestuffs, named after John Mercer, where a concentrated alkaline solution is used, such as sodium hydroxide (Clibbens, 1923; Yue et al., 2012).

2.2. X-ray diffraction

For characterizing the crystalline structure of the cotton samples, an X-ray machine (DRONEK 4-AXES, Huber Diffraktionstechnik GmbH & Co. KG, Germany) was used to conduct wide-angle X-ray diffraction (WAXD) under transmission mode on non-powder samples. Three 2θ line scans along the equatorial direction of the 2D X-ray diffraction pattern were carried out on each sample from 5° to 30° with the step of 0.2° and a counting time of 50 s. The X-ray was generated by Cu-Kα at 40 kV and 30 mA with a wavelength λ to be 0.154 nm. The intensity vs. 2θ curves were obtained by subtraction of a background scan carried out with no sample.

2.3. Thermogravimetric analysis

A TGA machine (STA 449 F3,NETZSCH-Gerätebau GmbH, Germany) was applied to perform the thermal stability analysis of the cotton samples from 30 °C to 650 °C with linear ramping speeds of 5, 10, 20 and 50 °C/min, under a Nitrogen purge gas of 40 ml/min. Each sample was cut into about 0.5 mm long short fibres, and the total weight was ca. 10 mg for each test, contained in 70 μL Al_2O_3 crucibles.

2.4. Determination of weight-average molecular weight and molecular weight distribution

The weight-average molecular weight (M_w), number-average molecular weight (M_n) and the molecular weight distribution (MWD) of the

natural cotton and the mercerized cotton samples were measured with the technique of multi-angle laser light scattering (MALLS), where the refractive index (RI) is used to determine the molecular weight (Andersson, Wittgren, & Wahlund, 2003; Yokoyama, Renner-Nantz, & Shoemaker, 1998). The solution used for injection was prepared as the following: First, the cotton samples were soaked in a water bath for 7 days at 40 °C before the solvent was exchanged from water to ethanol and finally into dimethylacetamide (DMAc). The samples were kept in the DMAc for 12 h and then fully dissolved in a 9 % solution of LiCl in DMAc. Each sample was measured twice. The method and results have been reported in our preceding paper (Liang, Ries, & Hine, 2022).

2.5. Determination of the contents of lignin and hemicellulose

First, the samples were cryogenically milled in a Retsch mill for 5–10 min and then thoroughly dried at 40 °C with a vacuum oven. In terms of the determination of the lignin content, the protocol of Iiyama and Wallis (Iiyama & Wallis, 1988) and the modification of Hatfield et al. (Hatfield, Grabber, Ralph, & Brei, 1999) were used on both the natural cotton and the mercerized cotton samples. Triplicate measurements were done on each sample. The analysis of the content of hemicellulose was performed in accordance to the acid methanolysis reported by Sundberg et al. (Sundheq, Sundherg, Lillandt, & Holmhom, 1996). The measurement of the contents of lignin and hemicellulose in the two samples have been reported in our preceding paper (Liang et al., 2022).

2.6. Theoretical considerations and calculation procedures for the pyrolysis analysis

The TGA data was analysed and modelled with a method modified from the simple FOG model and the equations related in the method are shown as:

$$\int_y^1 \frac{dy}{y^n} = \int_y^1 \frac{dy}{y} = \frac{A}{\beta} \int_{T_o}^T exp\left(-\frac{E}{RT}\right) dT \tag{8}$$

where y equals $1 - \alpha$, and the left-hand side could be integrated to be:

$$\int_y^1 \frac{dy}{y^1} = ln\left(\frac{1}{y}\right) \tag{9}$$

As the right-hand side of Eq. (8) cannot be integrated simply, approximations have to therefore be applied for its integration. When T is very close to the temperature of maximum pyrolysis speed, T_m, whose value can be confirmed from derivative thermogravimetry (DTG) curves, three approximations have previously been reported (Broido, 1969):

$$exp\left(-\frac{E}{RT}\right) \approx \left[\left(\frac{T}{T_m}\right)e^{-1}\right]^{\frac{E}{RT_m}} \tag{10}$$

$$exp\left(-\frac{E}{RT}\right) \approx exp\left[-\frac{E}{RT_m}*\left(2 - \frac{T}{T_m}\right)\right] \tag{11}$$

$$exp\left(-\frac{E}{RT}\right) \approx \left(\frac{T_m}{T}\right)^2 exp\left(-\frac{E}{RT}\right) \tag{12}$$

The three approximations yield three integration results, respectively

$$ln\left[ln\left(\frac{1}{y}\right)\right] = \left(\frac{E}{RT_m} + 1\right)lnT + C_1 \tag{13}$$

$$ln\left[ln\left(\frac{1}{y}\right)\right] = \frac{E}{RT_m^2}*T + C_2 \tag{14}$$

$$ln\left[ln\left(\frac{1}{y}\right)\right] = -\frac{E}{R}*\frac{1}{T} + C_3 \tag{15}$$

where C_1, C_2 and C_3 are constants, and slopes from the linear fittings ($\frac{E}{RT_m} + 1$, $\frac{E}{RT_m^2}$ and $-\frac{E}{R}$) can be used to calculate the activation energy. For the sake of simplicity, hereafter the three equations, Eqs. (13), (14) and (15), are referred to as the lnT, T and $\frac{1}{T}$ methods, respectively. These approximations are only valid when the temperature range is very close to T_m, otherwise wide temperature ranges will introduce non-negligible errors. Therefore, a modified FOG method is applied for the kinetic research on the pyrolysis of natural cotton and mercerized cotton samples, and more details will be given later.

3. Results and discussion

3.1. Crystalline structure

For analysing the composition of cellulose I and cellulose II in the samples, a deconvolution method (Liang et al., 2022; Liang, Hawkins, Ries, & Hine, 2021) was used where cellulose I and cellulose II peaks are deconstructed to subpeaks fitted with Gaussian functions, deconvolution results of the raw natural cotton and the raw mercerized cotton are shown in Fig. 1 (a) and (b) respectively. Diffraction peaks at 14.8°(110), 16.3° (1$\bar{1}$0) and 22.4 (200) are assigned to the cellulose I, and those at 12.4° (1$\bar{1}$0), 20.2° (110) and 21.8° (200) are from the cellulose II structure (Liu et al., 2012). It is worth noting that the cellulose I peak at 20.6° (120), cannot be observed on an equatorial scan of our non-powder samples which is therefore not further discussed in this research (De et al., 2019). There is also a broad peak centred at 2θ of 18.2° which is associated with the amorphous fraction. After deconvolution, the summation of area under each peak for different crystal forms was obtained via integration, and the fraction of area summation of each crystalline structure to the total is used for quantifying the crystallinity. It should be noted that this is not a measure of the absolute cellulose I and cellulose II crystallinity, but rather a quasi-quantitative measure of crystal structure changes with mercerization. The cellulose I, cellulose II and amorphous region fractions of NCY and MCY were found to be 65 %, 0 % and 35 %, and 40.7 %, 19.7 % and 39.6 %, respectively. So as expected, mercerization reduced the cellulose I fraction, and increased the cellulose II and amorphous fractions.

3.2. Thermogravimetric analysis of the two cotton samples

TGA was conducted to characterize the mass loss with time of the two cotton samples at different heating speeds (5, 10, 20 and 50 °C/min), and the results are shown in Fig. 2.

It can be shown from Fig. 2 (a) and (b) that every TGA curve presents a single decomposition stage after a tiny weight loss step, ca. 4 %, located at around 80 °C attributed to water loss, indicating a primary pyrolysis stage. For both of the NCY and MCY samples, the decomposition stage shifted to higher temperature ranges as the heating rate increased, see the derivative (DTG) curves in Fig. 2 (c) and (d). The shifting of the decomposition stage is caused by the transfer limitation of heat and mass, resulting in a temperature gradient inside the samples (Cortés & Bridgwater, 2015).

For NCY, the decomposition began at around 270 °C and continued until 390 °C, while for MCY, the decomposition temperature range was found to be from 310 °C to 410 °C. Fig. 2 (c) indicates that the maximum decomposition rate of NCY was at between 334.6 °C and 357.4 °C within the range of heating rates, which is lower than MCY, from 354.4 °C to 381.8 °C, shown in Fig. 2 (d). The temperature at the maximum decomposition rate, T_m, increased with heating rate, β, and in order to get the intrinsic temperature at the maximum decomposition rate, $[T_m]$, which is the T_m when $\beta = 0$, the dependence of T_m on β is plotted and shown in Fig. 2 (e). Examination of the plots suggests that T_m dramatically increased in the beginning until it reached a plateau, and this applies to both sample cases. Therefore, we propose an exponential fitting equation to do modelling of the two datasets, expressed with the
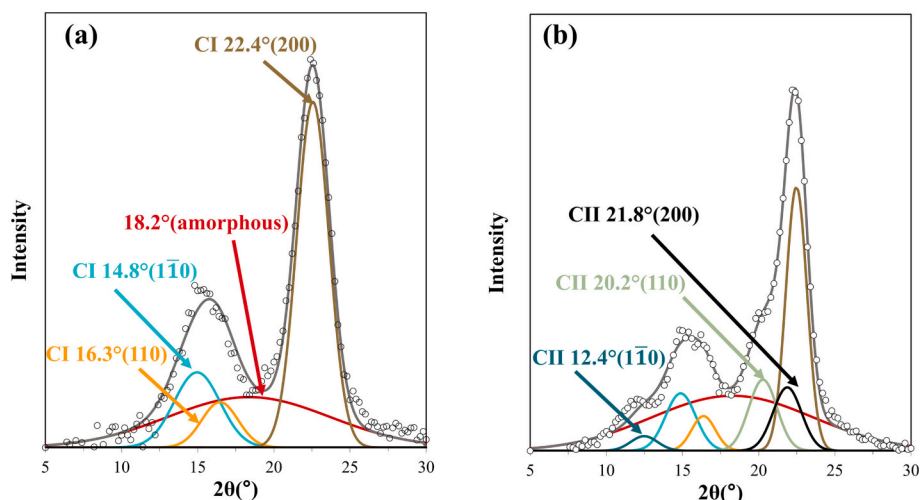
Fig. 1. WAXD spectrum deconvolution curves of (a) the natural cotton yarn and (b) the mercerized cotton yarn with relevant peaks labelled, where the open dots are the raw data, and the solid grey lines are summation of all deconvolution peaks, and CI and CII represent cellulose I and cellulose II respectively.
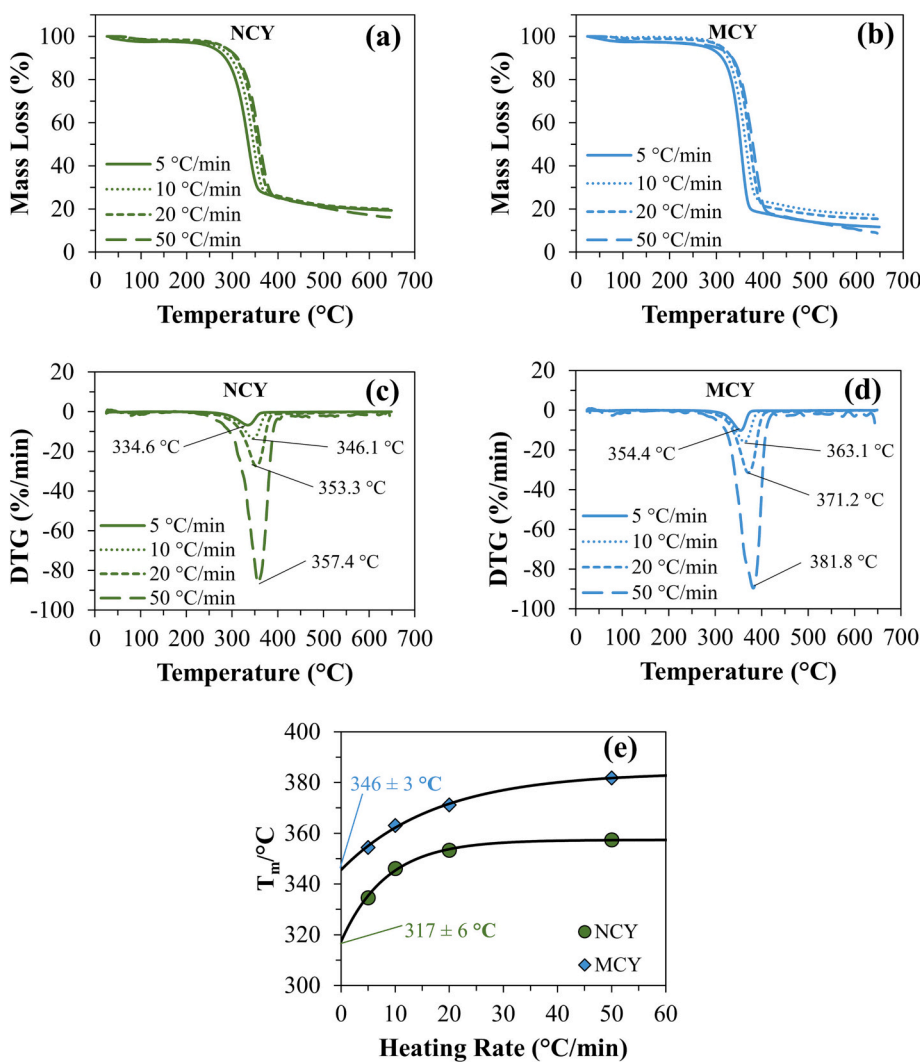
Fig. 2. Thermogravimetric analysis curves at different heating speeds for (a) the raw natural cotton yarn (NCY) and the raw mercerized cotton yarn (MCY); and derivative thermogravimetric (DTG) curves at different temperature ramping rates for (c) NCY and (d) MCY; (e) dependence of the temperature at the maximum decompositon rate (T_m) on the heating rate of TGA on both the samples, where the datasets are fitted with an exponential appoach equation (Eq. (16)) shown with the black solid lines with $R^2 > 0.99$.

equation below to determine T_m:

$$T_m = a \times \left(1 - e^{-b\beta}\right) + [T_m] \tag{16}$$

where a, b are constants, and $[T_m]$ can be confirmed from the intercept where the heating rate is zero, see Fig. 2 (c). The confidence of the fitting can be expressed with the coefficient of determination, R^2, which are

larger than 0.99 in both NCY and MCY datasets, giving $[T_m]$ to be 317 ± 6 °C and 346 ± 3 °C respectively.

3.3. Determination of the pyrolysis activation energy

As to the determination of the pyrolysis activation energy, it is essential to choose the suitable modelling method. Here, two methods are compared regarding their applicability and reliability on the two cotton samples, based on the conditions applied on the TGA measurements - the FOG method belonging to the model-fitting method, and the Friedman method, a model-free method or the isoconventional method. According to Eqs. (6) and (8), both are dependent on the heating rate, β, and even though the heating rate was set to be a constant on the machine when measuring, in reality it might not be. So, it is essential to quantify the actual heating rate during the measurement, therefore the instantaneous heating rate (β') is introduced and expressed by Eq. (17) below:

$$\beta' = \frac{T_n - T_{n-1}}{t_n - t_{n-1}} \tag{17}$$

where T_n, and T_{n-1} measure the nth temperature and the (n-1)th temperature of the TGA measurement range, and t_n and t_{n-1} represent the corresponding time at each temperature, respectively.

Fig. 3 shows the dependence of the instantaneous heating rate (β') with temperature for the two cotton samples, at different target heating rates.

As shown in Fig. 3, for both the NCY and MCY samples, the instantaneous heating rates were not constant with temperature, and it firstly increased to a temperature higher than the target and then dropped down to a steady value – close to the target heating rate (β_t), which does not conform to the assumptions applied in the FOG and Friedman method. As the target heating rate increases, the temperature at which the β' turns over increased, e.g. for 5 °C/min the turn-over temperature is ca. 80 °C, while as to 50 °C/min it becomes ca. 250 °C. A larger fluctuation can be found at higher target heating rates, and this can be further proved from the results shown in Table 2, where the higher the β_t is, the larger the difference between the maximum instantaneous heating rate (β_i^{max}) and the minimum instantaneous heating rate (β_i^{min}) is, and for the β_t of 50 °C/min the difference is large as ca. 100 °C/min.

Recall Eq. (7) for the Friedman method and Eq. (8) for the FOG method. The former relies more on β', as it is in a differential format depending on the instantaneous value of $\frac{d\alpha}{dt} = \frac{\beta d\alpha}{dT}$, but the latter relies on the average heating rate, $\overline{\beta_i}$, within the temperature range for the integration. $\overline{\beta_i}$ is expressed as

$$\overline{\beta_i} = \frac{\sum\limits_{j=1}^{n} \beta'(T_j)}{n} \tag{18}$$
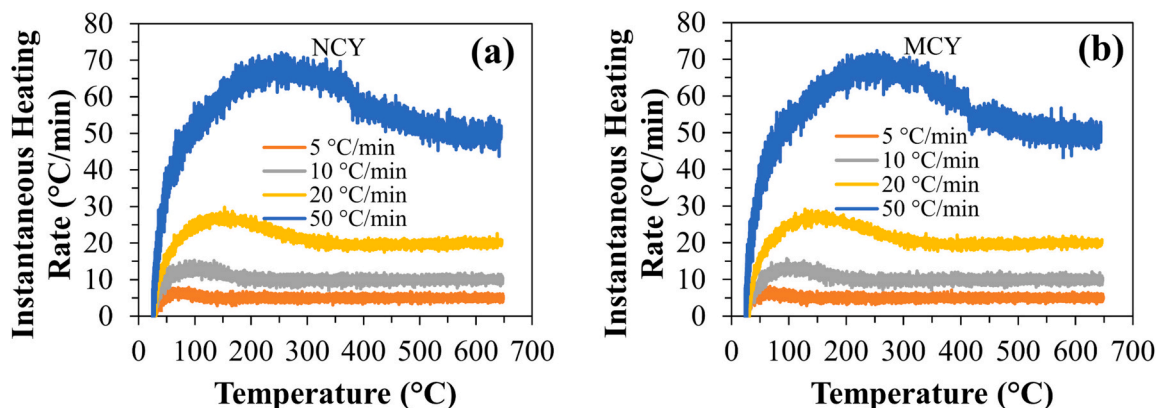
Table 2
Statistical results of instantaneous heating rate for the NCY and the MCY at different target heating rates set for TGA measurements.

Sample	Target heating rate (β_t) (°C/min)	Average instantaneous heating rate ($\overline{\beta_i}$) (°C/min)	Maximum instantaneous heating rate (β_i^{max}) (°C/min)	Minimum instantaneous heating rate (β_i^{min}) (°C/min)
NCY	5.0	5.0 ± 0.1	7.9	0.2
	10.0	10.0 ± 0.1	15.3	0.3
	20.0	20.0 ± 0.1	29.1	0.1
	50.0	50.0 ± 0.3	98.8	0.3
MCY	5.0	5.0 ± 0.1	8.1	0.8
	10.0	10.0 ± 0.1	15.7	0.3
	20.0	19.9 ± 0.1	29.1	0.2
	50.0	50.1 ± 0.3	100.9	0.3

$\overline{\beta_i}$ is calculated with Eq. (18).

where $\beta'(T_j)$ measures the instantaneous heating rate at temperature T_j.

Therefore, in our case - the temperature controlling ability of the TGA machine shown in Fig. 3 – the FOG method is more appropriate to be used for analysing the pyrolysis behaviour of the two cotton samples. However, the reliability of the approximations for the exponential term on the right-hand side of Eq. (8) needs to be further proved, see Eqs. (10), (11) and (12).

To examine the discrepancy of the three approximations from the exact result, the difference between them within the measuring temperature range is analysed, see Fig. 4, where the difference, Δ, is calculated, according to the integration result of the left-hand side (I_L) and the right-hand side (I_R) of the comparison item shown in each plot in Fig. 4, through the equation below:

$$\Delta = \frac{|I_L - I_R|}{I_L} \times 100\% \tag{19}$$

The values used for the simulation in Fig. 4 come from ranges of the corresponding values for the cellulose pyrolysis reported in the literature. These have been reported as 135 to 223 kJ/mol for the range of activation energies and 300 to 400 °C for the range of temperatures at maximum decomposition rate. From the simulated results shown in Fig. 4, the discrepancy decreases as the temperature increases until the temperature of the maximum decomposition rate (T_m=619 K (346 °C)), where the discrepancy reaches the lowest value in all the three cases. After that, the discrepancy bounces back and increases with temperature. This suggests that as the temperature gets close to T_m, the discrepancy is smaller and the more reliable is the approximation. In terms of the different approximations, the discrepancy of the approximation in Eq. (10) is very close to that in Eq. (11), both at <2 %, and

Fig. 3. Dependence of the TGA instantaneous heating rate (β') on tempearture for (a) the natural cotton yarn (NCY) and (b) the mercerized cotton yarn (MCY), where the legends represnt target heating rates set on the TGA machine.
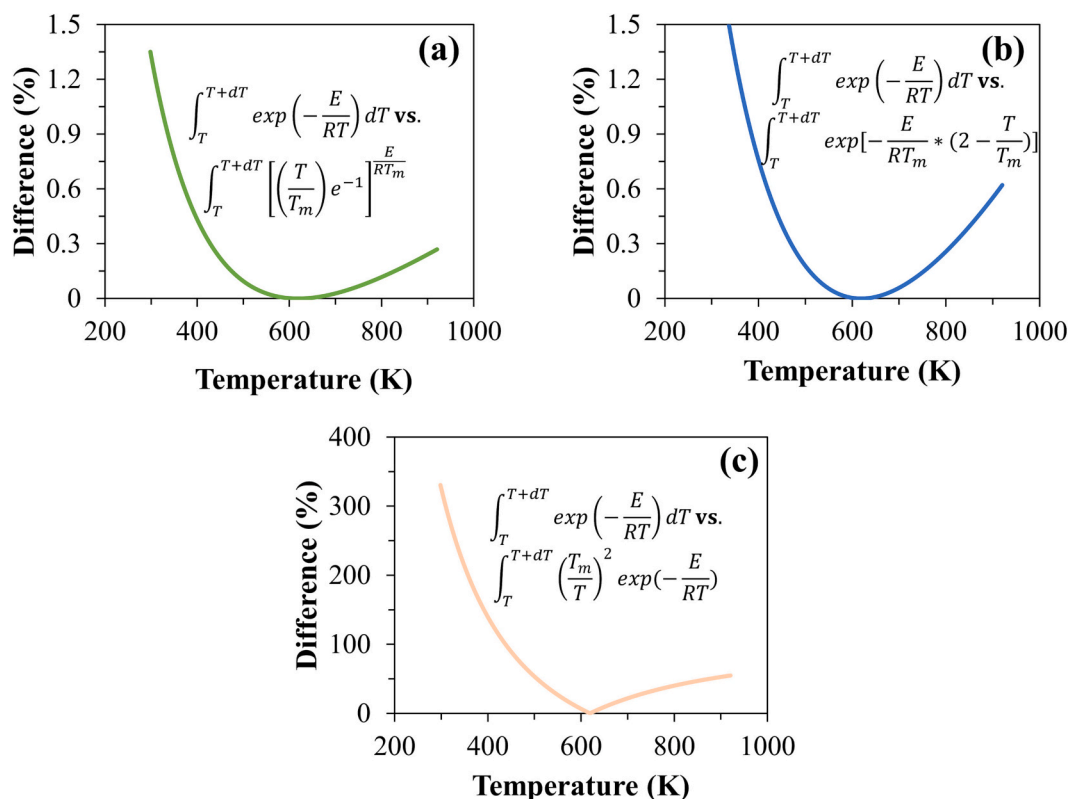
Fig. 4. Discrepancy analysis of the approximations from the exact result based on the first order global method (Eqs. (10), (11) and (12)),with the computing parameters of E, T_m and R to be 200 kJ/mol, 619 K (346 °C) and 8.314 J/(K.mol), respectively.

they are significantly smaller than that in Eq. (12) which could be large as 300 %. In order to decrease the discrepancy of the approximations of the FOG method, and to improve the reliability and applicability, the temperature ranges applied to the integrations shown in Eqs. (13), (14) and (15) need to be narrowed down to the temperature at the maximum decomposition rate, T_m.

Therefore, the FOG method needs to be modified to overcome the large discrepancy caused by the wide temperature range. Here we develop a modified FOG method to get the pyrolysis activation energy by gradually narrowing the temperature range centred at T_m, which can be confirmed from the DTG plots in Fig. 2, for lnT, T and $\frac{1}{T}$ methods. A series of temperature ranges are adopted in the approximations to calculate the pyrolysis activation energy with the method introduced earlier, for each sample at each target heating rate, and the dependence of pyrolysis activation energy as a function of the temperature range can be obtained, after which the tendency is used for further analysis. A practical example of how to get the pyrolysis activation energy for NCY at the heating rate of 50 °C/min is shown in Fig. 5. The pyrolysis activation energy can be obtained as follows. To begin, a series of temperature ranges for the integration of each of the three equations, Eqs. (13), (14) and (15), are chosen to be ±10 %, ± 5 %, ± 3 % and ± 1 % of T_m. Then, in order to get the pyrolysis activation energy from different approximations, a linear fitting is applied to each plot of $ln(ln(1/y))$ vs. the temperature item, $ln(T)$ for Eq. (13), T for Eq. (14) and 1000/T for Eq. (15), for every temperature range, see the doted lines in Fig. 5; the gradient of each line can be measured with the LINEST regression function in EXCEL.

Recall the method introduced in Section 2.6, the pyrolysis activation energies associated with temperature ranges and approximations are calculated with the equations below:

$$E_{lnT}^i = \left(G_{lnT}^i - 1\right) \times RT_m \tag{20}$$

$$E_T^i = G_T^i \times RT_m^2 \tag{21}$$

$$E_{1/T}^i = -G_{1/T}^i \times R \tag{22}$$

where G_{lnT}^i, G_T^i and $G_{1/T}^i$ measure the gradients of the straight lines according to Eqs. (13), (14) and (15) respectively, and correspondingly E_{lnT}^i, E_T^i and $E_{1/T}^i$ represent the pyrolysis activation energies; the superscript i means one of the temperature ranges of ±10 %, ±5 %, ±3 % and ±1 %. The dependence of the pyrolysis activation energy as a function of the temperature range at different target heating rates is shown in Fig. 6. These results indicate that the pyrolysis activation energy increased as the temperature range decreased, e.g. for the NCY, it increased from 119.0 ± 0.5 kJ/mol to 143.0 ± 0.1 kJ/mol when the temperature range decreased from ±10 % to ±1 % at the target heating rate of 5 °C/min (the dataset in orange in Fig. 6 (a)). Recall, the difference between the approximation and the exact result decreases as the temperature range decreases, see Fig. 4. Therefore, we develop a method to determine the pyrolysis activation energy when the temperature range tends to zero, and hereafter it is called the intrinsic pyrolysis activation energy ([E]), as follows. First, by examination, the quadratic equation was found to adequately match the dependence of pyrolysis activation energy as a function of temperature range with the determination coefficient $R^2 > 0.99$, shown in Fig. 6; by extrapolating the temperature range to zero, at which the difference between the approximation and exact result is minimised, corresponding to the lowest points of Fig. 4, the intrinsic pyrolysis activation energy was confirmed to be the constant item of the quadratic fitting line, using the advanced LINEST regression function in EXCEL.

The results in Fig. 6 are further tabulated in Table S1, indicating that there is not much difference in the intrinsic pyrolysis activation energy among the three approximations when the measurement was conducted under the same target heating rate (β_t), giving an average intrinsic
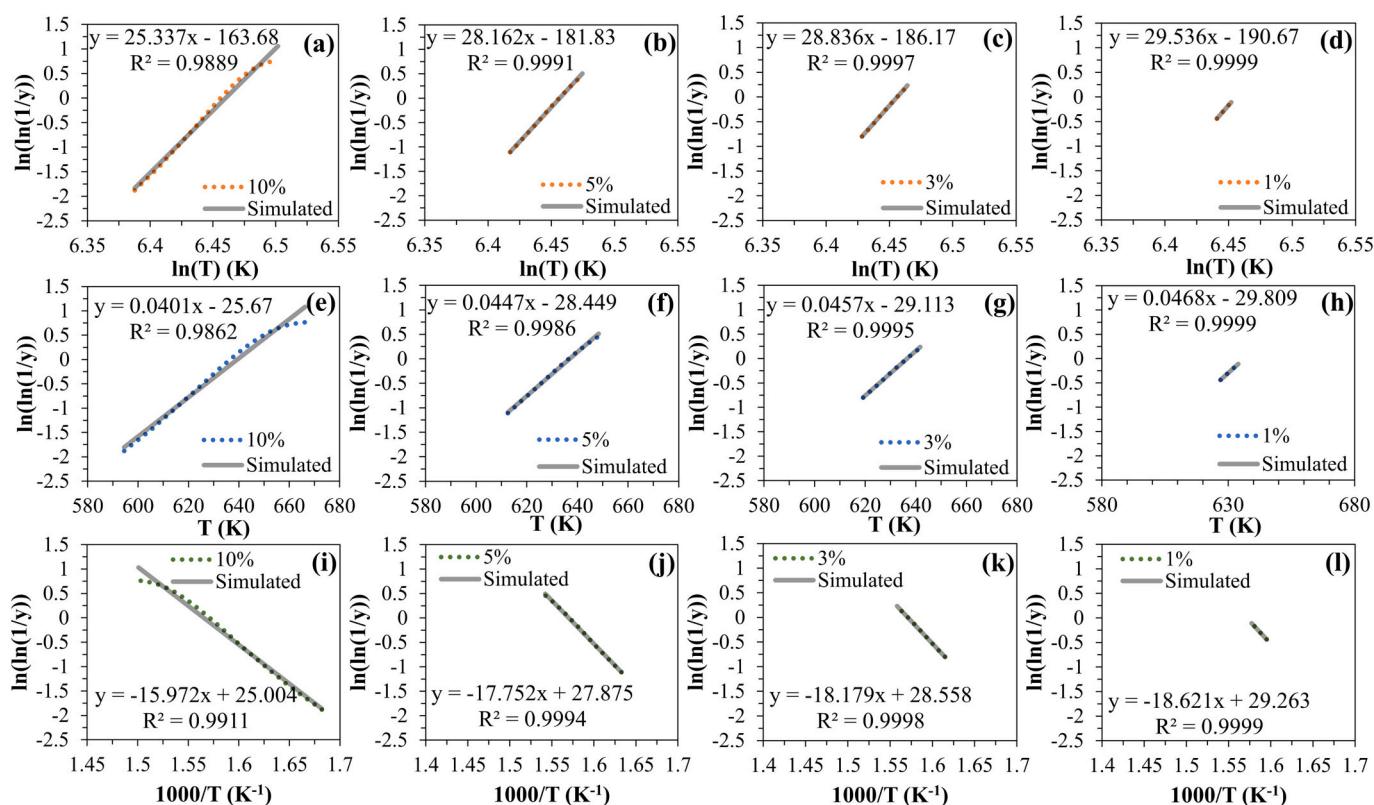
Fig. 5. Plots of $ln(ln(1/y))$ as a function of $ln(T)$ within the temperature ranges of (a) $\pm$ 10 %, (b) $\pm$ 5 %, (c) $\pm$ 3 % and (d) $\pm$ 1 % of the temperature of the maximum decompsition speed (T_m), based on Eq. (13); $ln(ln(1/y))$ as a function of T within the temperature ranges of (e) $\pm$ 10 %, (f) $\pm$ 5 %, (g) $\pm$ 3 % and (h) $\pm$ 1 % of the T_m, based on Eq. (14); $ln(ln(1/y))$ as a function of T within the temperature ranges of (i) $\pm$ 10 %, (j) $\pm$ 5 %, (k) $\pm$ 3 % and (l) $\pm$ 1 % of the T_m, based on Eq. (15), and all the data are for the natural cotton yarn measured with the target heating rate of 50 °C/min.

pyrolysis activation energy, $\overline{\left[E_{\beta_t}\right]}$, to be confirmed for each β_t. An independence of $\overline{\left[E_{\beta_t}\right]}$ on β_t is found on both the NCY and the MCY samples, and the former has a lower $\overline{\left[E_{\beta_t}\right]}$ than the later at each β_t.

To further analyse the dependence of $\overline{\left[E_{\beta_t}\right]}$ on samples and heating rates β_t, the plot of $[E_{\beta_t}]$ against β_t for both the cotton samples is produced and is shown in Fig. 7. For the NCY sample, the $\overline{\left[E_{\beta_t}\right]}$ obtained at different β_t are very close to each other, suggesting its independence of β_t and giving a mean value of the average intrinsic pyrolysis activation energy, $\overline{[E]}_{NCY}$, to be 153 $\pm$ 2 kJ/mol, see the solid green circles and the green dash line in Fig. 7. As for the MCY sample, a similar phenomenon is found that its $\overline{\left[E_{\beta_t}\right]}$ shows independence of β_t, therefore its mean value of the average intrinsic pyrolysis activation energies was calculated to be $\overline{[E]}_{MCY}$=192 $\pm$ 7 kJ/mol. This independence of pyrolysis activation energies on β_t proves the applicability and reliability of the modified FOG method to the samples under the conditions conducted for the TGA measurements in this study. It is important to note that the intrinsic pyrolysis activation energy determined in this article is at the temperature of the maximum decomposition speed.

Compared with NCY, MCY has about 23 % higher pyrolysis activation energy, and this result is consistent with the decomposition temperature analysis result shown in Fig. 2, suggesting the mercerized cotton is more thermally stable compared to the natural cotton. The pyrolysis activation energies, $\overline{[E]}_{NCY}$=153 $\pm$ 2 kJ/mol for the natural cotton yarn and $\overline{[E]}_{MCY}$=192 $\pm$ 7 kJ/mol for the mercerized cotton yarn, compare to the pyrolysis activation energies reported by Morgado, et al., at 158 kJ/mol and 187 kJ/mol for untreated cotton linters and mercerized cotton linters, respectively (Morgado & Frollini, 2011), and the pyrolysis activation energies of hemicellulose and lignin are reported to be within the ranges from 115 to 144 kJ/mol and from 23 to

108 kJ/mol, respectively (Zhu & Zhong, 2020). The higher pyrolysis activation energy and decomposition temperature seen in the mercerized cotton sample is likely due to the existing cellulose II with higher thermostability, found in the MCY. But further analysis of carbohydrate composition and molecular weight is needed, and therefore is discussed later.

3.4. Understanding the difference in pyrolysis activation energy between the two cotton samples

In order to investigate the reasons for the different pyrolysis activation energies found from the two samples, carbohydrate composition analysis and the MALLS/RI measurement for the molecular weight are conducted, and their results are shown in Table 3; the molecular weight distribution is shown in Fig. S1. Part of these analysis results have been reported in our preceding paper (Liang et al., 2022).

As shown in Table 3, the lignin content in the NCY, at 1.29 %, was slightly higher than that in the MCY, at 1.04 %. Carbohydrate composition resultants of hemicellulose were detected in the NCY sample, while they were not detectable in the MCY sample, which means the mercerization process removed some lignin and all/most the hemicelluloses from the cotton samples. These results in combination with the results from the WAXD spectra in Fig. 1 indicate the effect of the mercerization process.

As for the molecular weights including M_n, M_w and MWD, the NCY sample is about 2.5 times higher than the MCY sample in the molecular weights, and also shows a slightly larger dispersity, see Table 3 and Fig. S1. This is likely due to the fact that the mercerization process degrades the cellulose molecules and reduces the low molecular weight carbohydrate polymers, i.e. the hemicellulose, which is consistent with the results of carbohydrate composition analysis showing no detectable
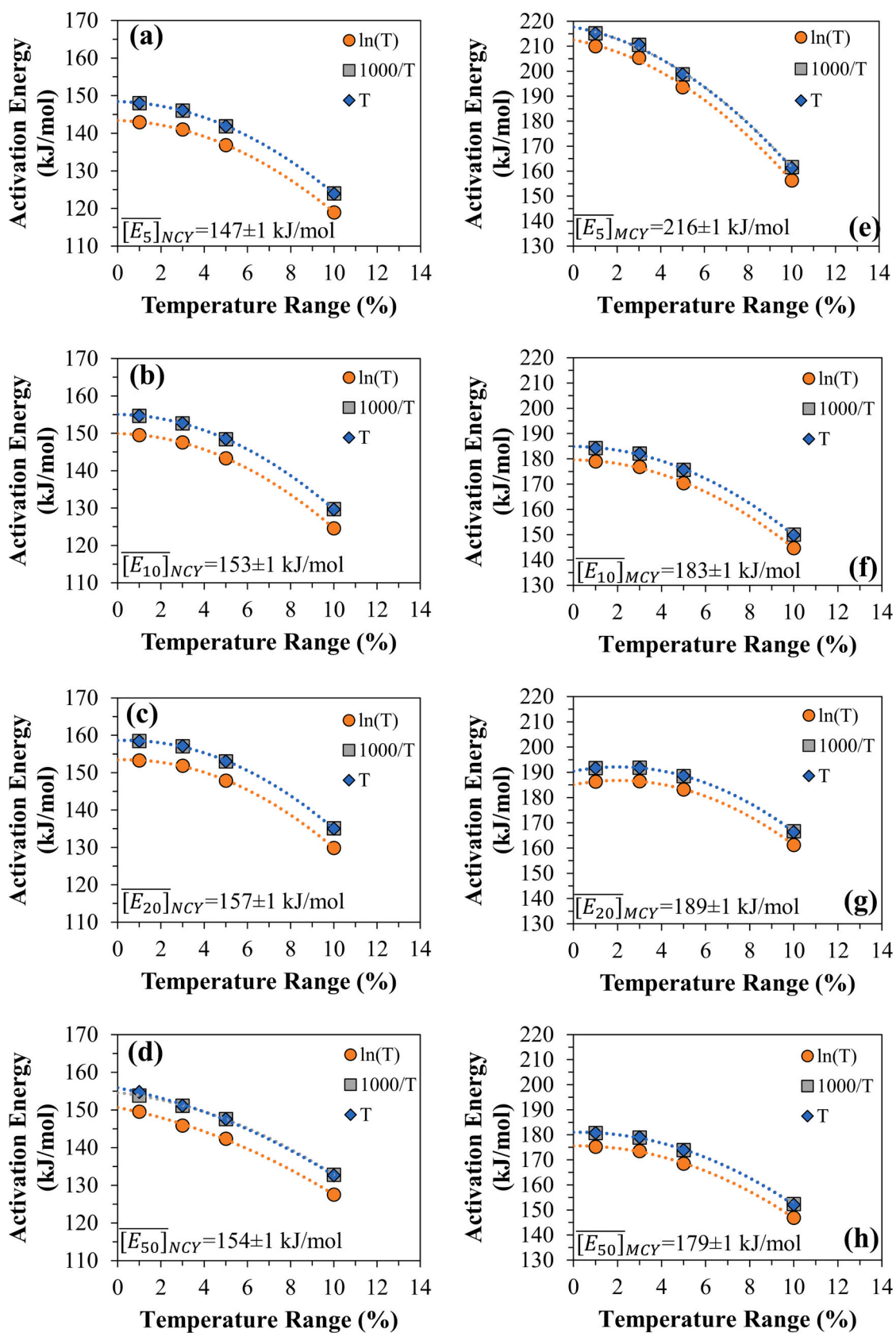
Fig. 6. Pyrolysis activation energy dependence of temperature range applied to the integration, where (a)–(d) are for the natural cotton yarn (NCY) measured at the target heating rate of 5, 10, 20 and 50 °C/min respectively, and (e)–(h) are for the mercerized cotton yarn (MCY) measured at different target heating rates of 5, 10, 20 and 50 °C/min, respectively. The dot lines are quadratic fitting results with $R^2 > 0.99$.
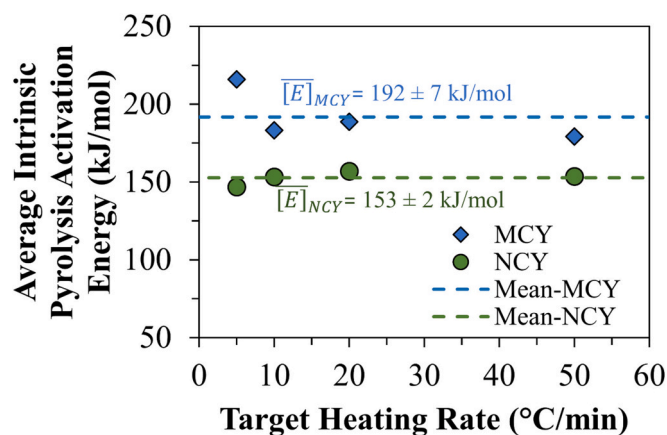
Fig. 7. Plot of average intrinsic pyrolysis activation energy ($\overline{[E_{\beta_t}]}$) vs. target heating rate (β_t) for the natural cotton yarn (NCY) and themercerized cotton yarn (MCY), where the dash lines show the locations of the mean values ($\overline{[E]}_{NCY}$ and $\overline{[E]}_{MCY}$).

Table 3

Comparison of the natural cotton yarn and the mercerized cotton yarn in carbohydrate composition, including lignin and hemicellulose, and molecular weight. Table taken and adapted from the paper of Liang et al. (Liang et al., 2022).

Property	NCY	MCY
Lignin content of dry samples (%)	1.29	1.04
Arabinose (mg/g)	3.94	null
Rhamnose (mg/g)	1.23	null
Xylose (mg/g)	2.08	null
Galacturonic acid (mg/g)	6.73	null
Mannose (mg/g)	null	null
Galactose (mg/g)	2.72	null
Glucose (mg/g)	156.69	142.95
M_n (kDa)	653 ± 18	252 ± 5
M_w (kDa)	1069 ± 19	385 ± 4
Polydispersity [M_w/M_n]	1.64 ± 0.07	1.53 ± 0.02
Reg (μmol/g)	1.53 ± 0.04	3.98 ± 0.09

NB: the glucose contents in the table are from the hemicellulose in our samples, as reported by Sundberg et al.

hemicellulose in the MCY sample. It could also be due to the different plant source for the raw cotton before it was mercerized.

In combination with the carbohydrate-compositional analysis and XRD results, the reasons for the difference in pyrolysis activation energy between NCY and MCY are hypothesized. The existence of hemicellulose, with lower pyrolysis activation energy than cellulose, in the NCY sample shifted the apparent pyrolysis activation energy to a lower value; and the thermal stability of cellulose II existing in MCY is higher than that of cellulose I, the only cellulose crystalline structure in NCY. Besides, even though the molecular weight of NCY is higher than that of MCY, the thermal stability of NCY is worse than that of MCY, with lower decomposition temperature and pyrolysis activation energy, suggesting that the molecular weight plays a more minor role in the thermal stability of cellulose-base materials, while the carbohydrate composition and crystalline structure dominate, when non-cellulose lignocellulose materials existing, i.e. hemicellulose and lignin.

4. Conclusions

The pyrolysis kinetics of the cellulose-based materials, the natural cotton yarn and the mercerized cotton yarn, have been successfully investigated via TGA. In addition to help understand and interpret the results, X-ray scattering, chemical composition analysis and MALLS/RI are implemented to explore the other comparative properties, i.e. the crystalline structure, contents of hemicellulose and lignin, and molecular weight, respectively. The examination of the instantaneous actual heating rate showed a large discrepancy from the target heating rate, indicating that the FOG method could be more suitable than those iso-conventional methods, as the later relies on the instantaneous actual heating rate, by contrast the former is more average heating rate dependant. Three approximations were applied to the FOG method, of which the discrepancy from the origin formula is found to be improved with the decrease of the integral temperature range. The decomposition temperature was found dependent of the applied heating rate, and the intrinsic decomposition temperature, at heating rate of 0 °C/min, was determined to be 317 ± 3 °C of NCY and 346 ± 6 °C of MCY. On the contrary, the pyrolysis activation energy is found to be independent of the heating rate, giving average values of 153 ± 2 kJ/mol and 192 ± 7 kJ/mol for NCY and MCY, respectively, which is in line with the literature (Morgado & Frollini, 2011). The higher thermal stability of the MCY than NCY is hypothesized to be because the existence of hemicellulose in the NCY lowers the decomposition temperature and the pyrolysis activation energy, and the cellulose II, with higher thermal stability than cellulose I, exists in MCY. The findings, i.e. the modified FOG method can provide a new approach in the investigation on pyrolysis kinetics of biomass and help understand the factors impacting the pyrolytic behaviour of other cellulose-based materials.

CRediT authorship contribution statement

Yunhao Liang: Conceptualization, Methodology, Investigation, Writing – original draft, Visualization. **Michael E. Ries:** Supervision, Conceptualization, Writing – review & editing, Project administration. **Peter J. Hine:** Supervision, Conceptualization, Writing – review & editing, Project administration.

Declaration of competing interest

The authors declare that they have no known competing financial interests or personal relationships that could have appeared to influence the work reported in this paper.

Data availability

Data will be made available on request.

Appendix A. Supplementary data

Supplementary data to this article can be found online at https://doi.org/10.1016/j.carbpol.2022.120518.

References

Andersson, M., Wittgren, B., & Wahlund, K.-G. (2003). Accuracy in multiangle light scattering measurements for molar mass and radius estimations. Model calculations and experiments. *Analytical Chemistry, 75*(16), 4279–4291. https://doi.org/10.1021/ac030128+

Banyasz, J. L., Li, S., Lyons-Hart, J. L., & Shafer, K. H. (2001). Cellulose pyrolysis: The kinetics of hydroxyacetaldehyde evolution. *Journal of Analytical and Applied Pyrolysis, 57*(2), 223–248. https://doi.org/10.1016/S0165-2370(00)00135-2

Broido, A. (1969). A simple, sensitive graphical method of treating thermogravimetric analysis data. *Journal of Polymer Science Part A-2: Polymer Physics, 7*(10), 1761–1773. https://doi.org/10.1002/pol.1969.160071012

Cao, W., Li, J., Martí-Rosselló, T., & Zhang, X. (2019). Experimental study on the ignition characteristics of cellulose, hemicellulose, lignin and their mixtures. *Journal of the Energy Institute, 92*(5), 1303–1312. https://doi.org/10.1016/j.joei.2018.10.004

Chen, W.-H., & Kuo, P.-C. (2011). Isothermal torrefaction kinetics of hemicellulose, cellulose, lignin and xylan using thermogravimetric analysis. *Energy, 36*(11), 6451–6460. https://doi.org/10.1016/j.energy.2011.09.022

Clibbens, D. A. (1923). XII.—THE MERCERISATION OF COTTON: A review of the literature. Journal of the textile institute. *Transactions, 14*(8), T217–T249.

Coats, A. W., & Redfern, J. P. (1964). Kinetic parameters from thermogravimetric data. *Nature, 201*(4914), 68–69. https://doi.org/10.1038/201068a0

Cortés, A. M., & Bridgwater, A. V. (2015). Kinetic study of the pyrolysis of miscanthus and its acid hydrolysis residue by thermogravimetric analysis. *Fuel Processing Technology, 138*, 184–193. https://doi.org/10.1016/j.fuproc.2015.05.013

Czajka, K. M. (2021). The impact of the thermal lag on the interpretation of cellulose pyrolysis. *Energy, 236*, Article 121497. https://doi.org/10.1016/j.energy.2021.121497

De, C., Giannini, Lassandro, Scattarella, Sibillano, Matricciani, & Fanti. (2019). X-ray dating of ancient linen fabrics. *Heritage, 2*(4), 2763–2783. https://doi.org/10.3390/heritage2040171

Ding, Y., Huang, B., Li, K., Du, W., Lu, K., & Zhang, Y. (2020). Thermal interaction analysis of isolated hemicellulose and cellulose by kinetic parameters during biomass pyrolysis. *Energy, 195*, Article 117010. https://doi.org/10.1016/j.energy.2020.117010

Dussan, K., Dooley, S., & Monaghan, R. F. (2019). A model of the chemical composition and pyrolysis kinetics of lignin. *Proceedings of the Combustion Institute, 37*(3), 2697–2704. https://doi.org/10.1016/j.proci.2018.05.149

Fan, Y., Cai, Y., Li, X., Jiao, L., Xia, J., & Deng, X. (2017). Effects of the cellulose, xylan and lignin constituents on biomass pyrolysis characteristics and bio-oil composition using the simplex lattice mixture design method. *Energy Conversion and Management, 138*, 106–118. https://doi.org/10.1016/j.enconman.2017.01.075

Farag, S., Attia, M., & Mohaddespour, A. (2021). Model of the slow pyrolysis of lignin to predict the product yield and composition of the liquid phase. *Biofuels, Bioproducts and Biorefining, 15*(1), 163–175. https://doi.org/10.1002/bbb.2146

Friedman, H. L. (1964). Kinetics of thermal degradation of char-forming plastics from thermogravimetry. Application to a phenolic plastic. *Journal of Polymer Science Part C: Polymer Symposia, 6*(1), 183–195. https://doi.org/10.1002/polc.5070060121

Hatfield, R. D., Grabber, J., Ralph, J., & Brei, K. (1999). Using the acetyl bromide assay to determine lignin concentrations in herbaceous plants: Some cautionary notes. *Journal of Agricultural and Food Chemistry, 47*(2), 628–632. https://doi.org/10.1021/jf9808776

Iiyama, K., & Wallis, A. F. A. (1988). An improved acetyl bromide procedure for determining lignin in woods and wood pulps. *Wood Science and Technology, 22*(3), 271–280. https://doi.org/10.1007/BF00386022

Kim, U.-J., Eom, S. H., & Wada, M. (2010). Thermal decomposition of native cellulose: Influence on crystallite size. *Polymer Degradation and Stability, 95*(5), 778–781. https://doi.org/10.1016/j.polymdegradstab.2010.02.009

Leng, E., Guo, Y., Chen, J., Liu, S., EJ, & Xue, Y. (2022). A comprehensive review on lignin pyrolysis: Mechanism, modeling and the effects of inherent metals in biomass. *Fuel, 309*, 122102. https://doi.org/10.1016/j.fuel.2021.122102

Liang, Y., Hawkins, J. E., Ries, M. E., & Hine, P. J. (2021). Dissolution of cotton by 1-ethyl-3-methylimidazolium acetate studied with time–temperature superposition for three different fibre arrangements. *Cellulose, 28*(2), 715–727. https://doi.org/10.1007/s10570-020-03576-x

Liang, Y., Ries, M. E., & Hine, P. J. (2022). Three methods to measure the dissolution activation energy of cellulosic fibres using time-temperature superposition. *Carbohydrate Polymers, 291*, Article 119541. https://doi.org/10.1016/j.carbpol.2022.119541

Liu, H., Cheng, G., Kent, M., Stavila, V., Simmons, B. A., Sale, K. L., & Singh, S. (2012). Simulations reveal conformational changes of methylhydroxyl groups during dissolution of cellulose Iβ in ionic liquid 1-ethyl-3-methylimidazolium acetate. *The Journal of Physical Chemistry B, 116*(28), 8131–8138. https://doi.org/10.1021/jp301673h

Luo, L., Guo, X., Zhang, Z., Chai, M., Rahman, M. M., Zhang, X., & Cai, J. (2020). Insight into pyrolysis kinetics of lignocellulosic biomass: Isoconversional kinetic analysis by the modified friedman method. *Energy & Fuels, 34*(4), 4874–4881. https://doi.org/10.1021/acs.energyfuels.0c00275

Lv, D., Xu, M., Liu, X., Zhan, Z., Li, Z., & Yao, H. (2010). Effect of cellulose, lignin, alkali and alkaline earth metallic species on biomass pyrolysis and gasification. *Fuel Processing Technology, 91*(8), 903–909. https://doi.org/10.1016/j.fuproc.2009.09.014

Mamleev, V., Bourbigot, S., & Yvon, J. (2007). Kinetic analysis of the thermal decomposition of cellulose: The main step of mass loss. *Journal of Analytical and Applied Pyrolysis, 80*(1), 151–165. https://doi.org/10.1016/j.jaap.2007.01.013

Morgado, D. L., & Frollini, E. (2011). Thermal decomposition of mercerized linter cellulose and its acetates obtained from a homogeneous reaction. *Polímeros, 21*(2), 111–117. https://doi.org/10.1590/S0104-14282011005000025

Moriana, R., Zhang, Y., Mischnick, P., Li, J., & Ek, M. (2014). Thermal degradation behavior and kinetic analysis of spruce glucomannan and its methylated derivatives. *Carbohydrate Polymers, 106*, 60–70. https://doi.org/10.1016/j.carbpol.2014.01.086

Özsin, G. (2020). Assessing thermal behaviours of cellulose and poly (methyl methacrylate) during co-pyrolysis based on an unified thermoanalytical study. *Bioresource Technology, 300*, Article 122700. https://doi.org/10.1016/j.biortech.2019.122700

Poletto, M., Zattera, A. J., Forte, M. M. C., & Santana, R. M. C. (2012). Thermal decomposition of wood: Influence of wood components and cellulose crystallite size. *Bioresource Technology, 109*, 148–153. https://doi.org/10.1016/j.biortech.2011.11.122

Qu, G., He, W., Cai, Y., Huang, X., & Ning, P. (2016). Catalytic pyrolysis of cellulose in ionic liquid [bmim]OTf. *Carbohydrate Polymers, 148*, 390–396. https://doi.org/10.1016/j.carbpol.2016.04.052

Ramiah, M. (1970). Thermogravimetric and differential thermal analysis of cellulose, hemicellulose, and lignin. *Journal of Applied Polymer Science, 14*(5), 1323–1337. https://doi.org/10.1002/app.1970.070140518

Şerbănescu, C. (2014). Kinetic analysis of cellulose pyrolysis: A short review. *Chemical Papers, 68*(7), 847–860. https://doi.org/10.2478/s11696-013-0529-z

Shen, D. K., Gu, S., & Bridgwater, A. V. (2010). The thermal performance of the polysaccharides extracted from hardwood: Cellulose and hemicellulose. *Carbohydrate Polymers, 82*(1), 39–45. https://doi.org/10.1016/j.carbpol.2010.04.018

Stamm, A. J. (1956). Thermal degradation of wood and cellulose. *Industrial & Engineering Chemistry, 48*(3), 413–417. https://doi.org/10.1021/ie51398a022

Sundheq, A., Sundherg, K., Lillandt, C., & Holmhom, B. (1996). Determination of hemicelluloses and pectins in wood and pulp fibres by acid methanolysis and gas chromatography. *Nordic Pulp & Paper Research Journal, 11*(4), 216–219. https://doi.org/10.3183/npprj-1996-11-04-p216-219

Thanatawee, P., Rukthong, W., Sunphorka, S., Piumsomboon, P., & Chalermsinsuwan, B. (2016). Effect of biomass compositions on combustion kinetic parameters using response surface methodology. *International Journal of Chemical Reactor Engineering, 14*(1), 517–526. https://doi.org/10.1515/ijcre-2015-0082

Vanderfleet, O. M., Reid, M. S., Bras, J., Heux, L., Godoy-Vargas, J., Panga, M. K. R., & Cranston, E. D. (2019). Insight into thermal stability of cellulose nanocrystals from new hydrolysis methods with acid blends. *Cellulose, 26*(1), 507–528. https://doi.org/10.1007/s10570-018-2175-7

Wang, S. R., Dai, G. X., Yang, H. P., & Luo, Z. Y. (2017). Lignocellulosic biomass pyrolysis mechanism: A state-of-the-art review. *Progress in Energy and Combustion Science, 62*, 33–86. https://doi.org/10.1016/j.pecs.2017.05.004

Yaman, S. (2004). Pyrolysis of biomass to produce fuels and chemical feedstocks. *Energy Conversion and Management, 45*(5), 651–671. https://doi.org/10.1016/S0196-8904(03)00177-8

Yang, H., Yan, R., Chen, H., Lee, D. H., & Zheng, C. (2007). Characteristics of hemicellulose, cellulose and lignin pyrolysis. *Fuel, 86*(12), 1781–1788. https://doi.org/10.1016/j.fuel.2006.12.013

Yeo, J. Y., Chin, B. L. F., Tan, J. K., & Loh, Y. S. (2019). Comparative studies on the pyrolysis of cellulose, hemicellulose, and lignin based on combined kinetics. *Journal of the Energy Institute, 92*(1), 27–37. https://doi.org/10.1016/j.joei.2017.12.003

Yokoyama, W., Renner-Nantz, J. J., & Shoemaker, C. F. (1998). Starch molecular mass and size by size-exclusion chromatography in DMSO-LiBr coupled with multiple angle laser light scattering. *Cereal Chemistry, 75*(4), 530–535. https://doi.org/10.1094/CCHEM.1998.75.4.530

Yue, Y., Zhou, C., French, A. D., Xia, G., Han, G., Wang, Q., & Wu, Q. (2012). Comparative properties of cellulose nano-crystals from native and mercerized cotton fibers. *Cellulose, 19*(4), 1173–1187. https://doi.org/10.1007/s10570-012-9714-4

Zhang, G., Feng, Q., Hu, J., Sun, G., Evrendilek, F., Liu, H., & Liu, J. (2022). Performance and mechanism of bamboo residues pyrolysis: Gas emissions, by-products, and reaction kinetics. *Science of the Total Environment, 838*, Article 156560. https://doi.org/10.1016/j.scitotenv.2022.156560

Zhang, J., Luo, J., Tong, D., Zhu, L., Dong, L., & Hu, C. (2010). The dependence of pyrolysis behavior on the crystal state of cellulose. *Carbohydrate Polymers, 79*(1), 164–169. https://doi.org/10.1016/j.carbpol.2009.07.038

Zhu, L., & Zhong, Z. (2020). Effects of cellulose, hemicellulose and lignin on biomass pyrolysis kinetics. *Korean Journal of Chemical Engineering, 37*(10), 1660–1668. https://doi.org/10.1007/s11814-020-0553-y